Renewable Energy 256 (2026) 124344

Contents lists available at ScienceDirect

Renewable Energy

journal homepage: www.elsevier.com/locate/renene

Optimization of energy extraction from salinity gradient using full-scale pressure retarded osmosis systems with hollow fiber membrane modules

D. Suárez-Alfonso [a,*], A. Ruiz-García [a], M. Khayet [b,c]

[a] Department of Electronic Engineering and Automation, University of Las Palmas de Gran Canaria, Campus Universitario de Tafira, E-35017, Las Palmas de Gran Canaria, Spain

[b] Department of Structure of Matter, Thermal Physics and Electronics, Faculty of Physics, University Complutense of Madrid, Avda. Complutense s/n, 28040, Madrid, Spain

[c] Madrid Institute for Advanced Studies of Water (IMDEA Water Institute), Calle Punto Net N° 4, 28805, Alcalá de Henares, Madrid, Spain

ARTICLE INFO

Keywords:
Blue energy
Pressure retarded osmosis
Membranes
Energy harvesting
Renewable energy resources

ABSTRACT

Pressure-retarded osmosis (PRO) involves a high concentration solution that is circulated through a semipermeable membrane and used to draw water permeate from a lower concentration solution by osmosis. PRO is a membrane-driven process in which the chosen membrane module plays a significant role in energy harvesting. This study aims to evaluate the effect of flow rate, pressure and concentration of draw solutions (30–180 g L^{-1}) on the performance of a full-scale PRO process and by incorporating the characteristics of a 10-inch hollow fiber membrane module from Toyobo Company Ltd. A single-stage PRO system with up to 3 membranes in series in a pressure vessel was considered, and the consumption of the pumps and energy recovery devices were taken into consideration. The results show the optimal operating conditions that maximize net power while varying the draw solution concentration and pressure and both water stream flow rates. A net power density of 2.56 W m^{-2} was achieved for the concentration gradient of 179.5 g L^{-1}. The present work concludes that single-stage full-scale PRO systems would be energetically feasible, although the results obtained need to be compared with an experimental plant taking into account membrane tear and fouling.

1. Introduction

The growing global population faces many challenges such as water scarcity, energy generation and food security [1]. To address part of these challenges, power generation through the use of renewable energy sources (RES) such as wind, solar and wave is being promoted. One of the main drawbacks of these RES is their intermittent and unpredictable nature, making their large-scale integration challenging [2]. For this reason, the use of predictable RES, such as blue energy, has gained importance in recent years [3]. In a salinity gradient power (SGP) process, the mixing of two different streams (commonly freshwater and seawater) releases Gibbs free energy that can be harvested. SGP depends on the natural hydrological cycle, with precipitation replenishing freshwater sources including rivers that ultimately meet up with the ocean. Alternatively, natural hypersaline resources, including hypersaline lakes and salt domes, can be used, as well as saline streams from industrial processes [4]. Some technologies allow the generation of electrical energy from the osmotic gradient [5], with the most studied being reverse electrodialysis (RED) and pressure-retarded osmosis (PRO) [6]. In addition to water resources, another factor limiting the viability of these technologies is the characteristics of the membranes. PRO has generated a lot of curiosity and acquired a certain degree of popularity in recent times [7]. There are two main membrane module configurations that can be used on an industrial scale, spiral wound or rolled flat sheet and hollow fiber membrane modules (SWMMS and HFMMS, respectively) [8]. Considerable effort is being made to improve the properties of PRO membranes [9], since the viability of PRO plants depends, among others, on the properties of the membrane module [10]. Modeling, simulation and optimization studies of PRO systems [11,12] are key to estimate the feasibility of the process from an energy and cost point of view [13]. Such studies can even propose what improvements would be needed in the PRO modules to ensure the viability of the process [10].

1.1. PRO using spiral wound membrane modules

As mentioned above, one of the main factors influencing the viability of the PRO technology is the membrane characteristics, which is usually related to the configuration of the membrane module. Achilli

* Corresponding author.
E-mail address: daniel.alfonso@ulpgc.es (D. Suárez-Alfonso).

https://doi.org/10.1016/j.renene.2025.124344
Received 26 April 2025; Received in revised form 17 August 2025; Accepted 5 September 2025
Available online 17 September 2025

Nomenclature

Abbreviations

Exp.	Experimental
Max.	Maximum
Op.	Operating
Sim.	Simulation

Acronyms

BP	booster pump
CTA	cellulose triacetate
DS	draw solution
DP	draw pump
ECP	external concentration polarization
ERD	energy recovery device
FLS	flat sheet
FS	feed solution
FO	forward osmosis
FP	feed pump
HF	hollow fiber
HFMM	hollow fiber membrane module
ICP	internal concentration polarization
PRO	pressure-retarded osmosis
PV	pressure vessel
RES	renewable energy sources
RO	reverse osmosis
SW	spiral wound
SWMM	spiral wound membrane module
TFC	thin-film composite

Variables

A	water permeability coefficient (m Pa^{-1} s^{-1})
A_0	initial value of A (m Pa^{-1} s^{-1})
B	solute permeability coefficient (m s^{-1})
C	concentration (g L^{-1})
D_i	inner diameter of the fiber bundle (m)
d_h	hydraulic diameter of feed channel (m)
d_i	inner fiber diameter (m)
H	spacer height (m)
h	specific enthalpy (J kg^{-1})
L	length of the HFMM (m)
n	number of elements in series
PD	power density (W m^{-2})
P	power (W)
p	pressure (Pa or bar)
Q	flow (m^3 h^{-1} or m^3 s^{-1})
R	flux recovery percentage (%)
R_i	inner radius of the fiber bundle (m)
R_o	outer radius of the fiber bundle (m)
Re	Reynolds number
Sc	Schmidt number
S_f	structural parameter (μm)
Sh	Sherwood number
S_m	membrane surface (m^2)
T	temperature (°C or K)
v	velocity (m s^{-1})

Greek letters

$\Delta\pi$	osmotic pressure gradient (Pa or bar)
Δp	pressure gradient (Pa or bar)
η	performance
μ	dynamic viscosity (kg m^{-1} s)
π	osmotic pressure (Pa or bar)
ρ	density (kg m^{-3})
ε	porosity in feed channel

Subscripts

av	average
D	draw
F	feed
in	input
m	membrane
p	permeate
TB	turbine

et al. [14] carried out an experimental study involving a reverse osmosis (RO)-PRO system for low-energy desalination using SWMMs. When testing the PRO process alone, a maximum power density (PD) of 1.15 W m^{-2} was achieved with 1 SWMM. The conditions in terms of draw and feed concentrations ($C_{D,in}$ and $C_{F,in}$) were 34.8 g L^{-1} NaCl and 0 g L^{-1} NaCl, respectively, and draw and feed pressures ($p_{D,in}$ and $p_{F,in}$) were 4.83 bar and 1.24 bar, respectively. Gupta et al. [15] carried out an experimental study and used the acquired data to estimate the behavior of PD with changes in $C_{D,in}$ and $p_{D,in}$. The developed model estimated 3.29 W m^{-2} for a salinity gradient ($C_{D,in}$-$C_{F,in}$) of 60–1 g L^{-1} NaCl, and draw and feed flow rates ($Q_{D,in}$ and $Q_{F,in}$) of 1.1×10^{-2} m^3 h^{-1} and 7×10^{-3} m^3 h^{-1}, respectively. Lee et al. [16] tested the performance of an 8-inch diameter SWMM and obtained a PD of 1.77 W m^{-2} for $C_{D,in}$ = 35 g L^{-1}. O'Toole et al. [17] considered a prototype 8040 SWMM module and reached a net power of 120 kW and 152 kW arranging 4834 membrane elements in parallel and 3429 membrane elements in a 3:1 tiered system, respectively. Seawater was the draw and freshwater the feed solution. Benjamin et al. [18] carried out a simulation-based study and used a 2×10^{-3} m^2 membrane to validate the developed model. The authors then studied 30 different membrane types in order to evaluate how the PRO system would function with each of them. Ranges of input parameters were $C_{D,in}$ = 27–66 g L^{-1}, $C_{F,in}$ = 0.26–27 g L^{-1}, and a maximum PD of 16.7 W m^{-2} was achieved with the SWMM used in [14].

Al-Zainati et al. [19] studied the impact of hydrodynamic conditions on optimum power generation in a dual-stage PRO system and simulated different membrane configurations (3 SWMMs in series in single-stage and also 3 elements in dual-stage). Arranging 2 SWMMs in series in the first stage and 1 SWMM in the second stage, the maximum specific energy generation (SEG) obtained was 0.68 kWh m^{-3} with a salinity gradient of 292.5–35.1 g L^{-1} NaCl. Matta et al. [20] carried out a simulation-based study and tried to predict the performance in terms of water flux and PD of some SWMMs. Using the membrane module of [21], a maximum PD of 9.8 W m^{-2} was obtained considering 160.29 g L^{-1} NaCl as the draw solution and seawater (35.1 g L^{-1} NaCl) as the feed solution. Ruiz-García et al. [22] provided a simulation tool for full-scale PRO systems using an 8-inch diameter SWMM. The optimal estimation was a maximum PD of 3.46 W m^{-2} and flux recovery (R) of 14.62% with 8 SWMMs in series. The salinity gradient was 50–0.5 g L^{-1}. Abdelkader et al. [23] who carried out a simulation-based study and proposed a novel design of an SWMM, obtained almost 4 W m^{-2} with it. The conditions were $C_{D,in}$ = 60 g L^{-1}, $C_{F,in}$ = 0.58 g L^{-1}. The use of PRO advanced spacers for reducing the specific energy consumption in hybrid desalination was addressed by Ng et al. [24].

The optimal PD obtained was 15 W m^{-2}, using RO brine as the draw solution. The role of water permeability coefficient (A) and solute permeability coefficient (B) in energy generation by PRO was also studied by Ruiz-García et al. [25]. Various ranges of A and B were considered. The simulated PRO system comprised 1 to 8 SWMMs in series, and the maximum power generation by the turbine was 1019.28 W for $C_{D,in}$ = 30 g L^{-1} and $C_{F,in}$ = 0.5 g L^{-1}. Tagliavini et al. [26] carried out a simulation-based study to quantify the effects of feed pre-treatment on net power generation. The authors modeled two membrane modules of cellulose triacetate (CTA) and thin-film composite (TFC), respectively. For the CTA membrane, a maximum power of 143 W was obtained which dropped to 48 W when feed pre-treatment with an energy requirement of 100 Wh m^{-3} was used. For the TFC membrane, the values were 284 W and 94 W, respectively. The conditions were 8 SWMMs in series, $C_{D,in}$ = 35.1 g L^{-1} and $C_{F,in}$ = 0.59 g L^{-1}. Ruiz-García et al. [10] carried out a simulation-based study to maximize the power generation of 1–8 full-scale SWMMs arranged in series using hypersaline draw solutions. Changes of the membrane permeability coefficients were also taken into account. The optimal value was a power estimation of 1777.33 W for 8 SWMMs in series, and a salinity gradient of 180-0.5 g L^{-1}. AL-Musawi et al. [27] studied three PRO scenarios with the objective of minimizing any environmental impact and promoting sustainable energy. Hypersaline solutions from RO brine were used as the draw solution and wastewater from demineralization processes as the feed solution. The authors reached 22.98 W of net power for $C_{D,in}$ = 51.8 g L^{-1}. In this study, the number of membrane modules arranged in series was not specified. Yagnambhatt et al. [28] carried out an experimental study by demonstrating the concept of real-time maximum power point tracking for an osmotic gradient power system. The membrane module used was flat sheet (FLS) and made of CTA. The maximum net power obtained was 2 W m^{-2} when considering a high concentration draw solution (RO-PRO system with energy recovery). The salinity gradient was 70-0 g L^{-1}. Also, a stand-alone PRO system was tested, and the authors reported a maximum PD of 0.2 W m^{-2}, for a variation of $C_{D,in}$ = 35 g L^{-1}. Summary information about the works described above, as well as membrane parameters such as A, B and membrane surface (S_m), can be found in the Table 1.

1.2. PRO using hollow fiber membrane modules

HFMMs are gaining prominence over SWMMs due to their higher packing density. Chou et al. [29] carried out an experimental study and reached a PD of 20.9 W m^{-2}, using synthetic seawater brine (58.5 g L^{-1} NaCl) as the draw solution and synthetic river water (0.06 g L^{-1} NaCl) as the feed solution. The developed membrane for this study was a TFC-polyetherimide HFMM. Sun et al. [30] carried out an experimental study with two TFC HFMMs. A maximum PD of 7.63 W m^{-2} was obtained, while the computed estimation indicated 9.54 W m^{-2}. $C_{D,in}$ was 58.5 g L^{-1} NaCl and DI water was the feed solution. Higa et al. [31] also performed an experimental study using a 5-inch diameter HFMM. The conditions were $C_{D,in}$ = 29.25 g L^{-1} and tap water as $C_{F,in}$. A maximum PD of 0.14 W m^{-2} was reached. An optimization study using 2 HFMMs of 5-inch diameter (by Toyobo Company Ltd.) considering seawater (35 g L^{-1}) as draw solution and pure water as feed solution was carried out by Kishimoto et al. [32]. Only 1 HFMM was considered. The optimal estimation was a maximum power production of 104 W per module with a PD of about 1.6 W m^{-2}.

Aseffa et al. [33] carried out a simulation-based study using Indian seawater (36 g L^{-1}) and riverwater (0.34 g L^{-1}) as draw and feed solutions, respectively. The authors achieved a maximum PD of 0.45 W m^{-2} (net power of 4.37 W). Matsuyama et al. [34] conducted an experimental study using a commercially available 10-inch diameter HFMM (HP10110EI-F1 by Toyobo Company Ltd.). A net PD of 2.8 W m^2 was achieved being the salinity gradient 35-0.2 g L^{-1}. Al-Zainati et al. [35] proposed a dual-staged RO and PRO hybrid system. Seawater with concentrations of 40 and 45 g L^{-1} were the RO feed solution and 1 g L^{-1} tertiary treated wastewater was the feed solution of the PRO process. The highest energy generation achieved by the PRO system was 79.3 kW at a 39% recovery rate. Low et al. [36] carried out an experimental evaluation of some TFC HFMMs at lab-scale and pilot-scale. The PD obtained in the lab-scale unit decreased from 9.1 W m^{-2} to 5.3 W m^{-2} with the increase of S_m. The conditions were $C_{D,in}$ = 58.5 g L^{-1} and DI water as $C_{F,in}$. Pilot scale evaluation of the 4-inch and 8-inch HFMMs resulted in lower PD of 2.5 W m^{-2} and 1.5 W m^{-2}, respectively. The conditions were $C_{D,in}$ = 58.5 g L^{-1} and DI water as $C_{F,in}$. Al-Zainati et al. [37] carried out a simulation-based study considering single, dual, ternary, and quaternary stages. A maximum PD of 15 W m^{-2} was obtained using seawater from the Dead Sea and wastewater ($C_{D,in}$ = 292.2 g L^{-1} and $C_{F,in}$ = 1.16 g L^{-1}). Summary information about the works described above, as well as membrane parameters such as A, B and S_m, can be found in the Table 2.

1.3. Hypersaline solutions and renewable energy production

The use of hypersaline solutions to generate electrical energy from the PRO process is attractive, since the higher the salinity gradient the more electrical energy can be generated. These solutions are available in certain geographical locations with hypersaline lakes or geothermal waters and in specific processes/industries where hypersaline solutions are generated [4]. Several authors have estimated the generation of electrical energy by the PRO process considering hypersaline aqueous solutions [4]. Emdadi et al. [38] studied electric energy production considering river discharge into the hypersaline Lake Urmia in Iran. The salinity of the lake is above 200 g L^{-1}. RED and PRO technologies were considered in the estimation of electric energy production. It was concluded that using PRO membranes with a PD of 5 W m^{-2} and a 10-year lifetime expectancy or 10 W m^{-2} and a 5-year lifetime expectancy the process would be viable. The authors did not determine the specific configuration of the PRO system or the optimal operating conditions. Madsen et al. [39] used two forward osmosis (FO) membranes to assess electric energy generation using the PRO technology. $C_{D,in}$ up to 290 g L^{-1} NaCl and Milli-Q water as feed solution were used. The variation of the A, B, S_f and PD for a range of $p_{D,in}$ was shown. A PD of about 30 W m^{-2} was reached for a $C_{D,in}$ = 175 g L^{-1} using the Hydration Technology Innovations (HTI, Albany, OR) CTA membrane. A techno-economic analysis of a PRO system for power production with hypersaline draw solution from the Great Salt Lake was carried out by Tran et al. [40]. The considered $C_{D,in}$ was 240 g L^{-1} and an estimation of the SEG of 4.5 kWh m^{-3} was claimed. This data was used to project a 25 MW PRO system. It was determined that the $Q_{D,in}$ and $Q_{F,in}$ needed were 5544 and 11088 m^3 h^{-1}, respectively. An RO-PRO system using HFMMs to reduce the specific energy consumption of the RO system using hypersaline solutions was proposed by Bargiacchi et al. [41]. The maximum PD obtained was about 0.6 W m^{-2} considering a hypothetical HFMM of 5 m in length, $C_{F,in}$ = 35 g L^{-1} and $C_{D,in}$ = 60 g L^{-1}. It was claimed that maximum values of PD were found for $\Delta p/\Delta\pi$ between 0.4 and 0.5. Janson et al. [42] conducted a techno-economic evaluation of a novel configuration that integrates PRO into the petroleum industry. The concentrations considered in this study were $C_{D,in}$ = 280 g L^{-1} and $C_{F,in}$ = 35 g L^{-1}. It was estimated that the maximum net energy generation was obtained for $p_{D,in}$ = 110 bar, far from the theoretical $\Delta\pi/2 \sim 80$ bar set elsewhere [43]. The maximum net energy generation value was 0.14 kWh m^{-3}. However, no characteristics of the membrane module used were specified.

1.4. Research gap and objectives

None of the above-mentioned studies have considered full-scale PRO systems with HFMMs. When considering full-scale systems, pressure losses on both sides along the membrane modules, as well as the dilution of the draw solution and the concentration of the feed solution, are considered. These factors (pressure losses on both sides, dilution

Table 1
Summary information on studies about PRO using SWMMs/FLS.

Reference	Max. PD	System characteristics	Salinity gradient	Op. Conditions
Achilli et al. [14]	1.15 W m^{-2} (Exp.)	S_m = 4.18 m^2	34.8-0 g L^{-1}	$p_{D,in}$ = 4.83 bar $p_{F,in}$ = 1.24 bar
Gupta et al. [15]	3.29 W m^2 (Sim. & Exp.)	S_m = 0.5 m^2 $A = 1.76 \times 10^{-12}$ m Pa^{-1} s^{-1} $B = 1.17 \times 10^{-7}$ m s^{-1}	60-1 g L^{-1}	$p_{D,in}$ = 21 bar $p_{F,in}$ = 0.2 bar $Q_{D,in} = 1.1 \times 10^{-2}$ m^3 h^{-1} $Q_{F,in} = 7 \times 10^{-3}$ m^3 h^{-1}
Lee et al. [16]	1.77 W m^{-2} (Sim. & Exp.)	S_m = 17.9 m^2	35-0.14 g L^{-1}	$p_{D,in}$ = 10.4 bar
O'Toole et al. [17]	0.84 W m^{-2} (Exp.)	Two-stages (3:1): 3429 membranes S_m = 53 m^2 $A = 1.42 \times 10^{-11}$ m Pa^{-1} s^{-1} $B = 2.4 \times 10^{-8}$ m s^{-1}	DS: Seawater FS: Freshwater	$p_{D,in}$ = 15.48 bar $p_{F,in}$ = 0.72 bar $Q_{D,in}$ = 0.97 m^3 h^{-1} $Q_{F,in}$ = 0.86 m^3 h^{-1}
O'Toole et al. [17]	0.47 W m^{-2} (Exp.)	Parallel sys. 4834 membranes S_m = 53 m^2 $A = 1.42 \times 10^{-11}$ m Pa^{-1} s^{-1} $B = 2.4 \times 10^{-8}$ m s^{-1}	DS: Seawater FS: Freshwater	$p_{D,in}$ = 14.05 bar $p_{F,in}$ = 0.38 bar $Q_{D,in}$ = 0.6 m^3 h^{-1} $Q_{F,in}$ = 0.54 m^3 h^{-1}
Benjamin et al. [18]	16.7 W m^{-2} (Sim.)	S_m = 4.18 m^2	$C_{D,in}$ = 27-66 g L^{-1} $C_{F,in}$ = 0.26-27 g L^{-1}	$Q_{D,in}$ = 720–8244 m^3 h^{-1}
Al-Zainati et al. [19]	680 Wh m^{-3} (Sim.)	S_m = 16.5 m^{-2}	292.5-35.1 g L^{-1}	$p_{D,in}$ = 108 bar $Q_{D,in}$ = 0.57 m^3 h^{-1}
Matta et al. [20]	9.8 W m^{-2} (Sim.)	$S_m = 2 \times 10^{-3}$ m^2 $A = 3.42 \times 10^{-12}$ m Pa^{-1} s^{-1} $B = 7.28 \times 10^{-7}$ m s^{-1} S_f = 689 μm	160.29-35.1 g L^{-1}	Not specified
Ruiz-García et al. [22]	3.46 W m^{-2} (Sim.)	8 elements in series S_m = 15.53 m^2 $A = 1.76 \times 10^{-12}$ m Pa^{-1} s^{-1} $B = 1.18 \times 10^{-7}$ m s^{-1}	50-0.5 g L^{-1}	$p_{D,in}$ = 22.5 bar $p_{F,in}$ = 2 bar $Q_{D,in}$ = 14.5 m^3 h^{-1} $Q_{F,in}$ = 6.5 m^3 h^{-1}
Abdelkader et al. [23]	4 W m^{-2} (Sim.)	S_m = 29 m^2 $A = 2 \times 10^{-12}$ m Pa^{-1} s^{-1} $B = 7.78 \times 10^{-8}$ m s^{-1}	60-0.58 g L^{-1}	Δp = 21 bar $Q_{D,in}$ = 1.35 m^3 h^{-1} $Q_{F,in}$ = 0.42 m^3 h^{-1}
Ng et al. [24]	15 W m^{-2} (Sim.)	S_m = 1 m^2 $A = 2.78 \times 10^{-12}$–2.5×10^{-11} m Pa^{-1} s^{-1} $B = 1.76 \times 10^{-7}$ m s^{-1} S_f = 100–1000 μm	DS: RO brine FS: Not specified	$p_{D,in}$ = 26 bar $p_{F,in}$ = 1.01 bar

(*continued on next page*)

Table 1 (*continued*).

Reference	Max. PD	System characteristics	Salinity gradient	Op. Conditions
Ruiz-García et al. [25]	3.14 W m^{-2} (Sim.)	1-8 elements in series S_m = 15.53, 20.53, 30.53, 40.53 m^2 $A = 2.12 \times 10^{-12}$–1.06×10^{-11} m Pa^{-1} s^{-1} $B = 5.55 \times 10^{-9}$–5.55×10^{-7} m s^{-1}	30-0.5 g L^{-1}	$p_{D,in}$ = 12 bar $Q_{D,in}$ = 12 m^3 h^{-1} $Q_{F,in}$ = 15.5 m^3 h^{-1}
Tagliavini et al. [26]	2.41 W m^{-2} (Sim.)	8 elements in series S_m = 14.75 m^2	35.1-0.59 g L^{-1}	$Q_{D,in}$ = 1.86 m^3 h^{-1} $Q_{F,in}$ = 2.46 m^3 h^{-1}
Ruiz-García et al. [10]	14.31 W m^{-2} (Sim.)	Single-stage: 1-8 elements in series S_m = 15.53 m^2 $A = 7.95 \times 10^{-12}$ m Pa^{-1} s^{-1} $B = 1.22 \times 10^{-7}$ m s^{-1} S_f = 446 μm	180-0.5 g L^{-1}	$p_{D,in}$ = 60 bar $p_{F,in}$ = 2 bar $Q_{D,in}$ = 3 m^3 h^{-1} $Q_{F,in}$ = 7.5 m^3 h^{-1}
AL-Musawi et al. [27]	2.84 W m^{-2} (Sim.)	S_m = 8.1 m^2	$C_{D,in}$ = 51.8 g L^{-1} FS: Not specified	Δp = 10.8 bar $Q_{D,in}$ = 0.9 m^3 h^{-1} $Q_{F,in}$ = 0.42 m^3 h^{-1}
Yagnambhatt et al. [28]	2 W m^{-2} (Exp.)	$S_m = 4.2 \times 10^{-3}$ m^2 $A = 1.17 \times 10^{-12}$ m Pa^{-1} s^{-1} $B = 1.11 \times 10^{-7}$ m s^{-1} S_f = 607 μm	70-0 g L^{-1}	Δp = 14 bar $Q_{D,in} = 4.3 \times 10^{-3}$ m^3 h^{-1} $Q_{F,in} = 3 \times 10^{-4}$ m^3 h^{-1}

of the draw solution and concentration of the feed solution) have a significant impact on the performance of this type of systems and cause changes in optimal operating conditions (i.e., operating conditions that maximize energy generation). The aim of this study was to evaluate the effect of the operating parameters on the performance of a single-stage industrial scale PRO process using HFMMs. The number of used HFMMs in series was between 1 and 3. The obtained optimal (maximizing the net energy generation) operating points were estimated using a simulation tool for PRO systems. This simulation tool allows to set boundary conditions and limitations in terms of flows, pressures and membrane characteristics to provide results as close to reality as possible.

2. Materials and methods

2.1. Mathematical model

The algorithm used in this study to estimate the performance of PRO systems has been previously published by the authors [22]. Almost all equations that are part of the mathematical model of the PRO process used in the present study can be found in the first sub-section of Supplementary material. It is worth noting that in the algorithm used, the membrane configuration considered was SWMM. Therefore, it was necessary to modify this algorithm to adapt it to HFMM. This was done by incorporating the following Eqs. (1), (2), (3) and (4):

$$Sh_D = 0.048 \cdot Re_D^{0.6} \cdot Sc_D^{\frac{1}{3}} \quad (1)$$

$$Sh_F = 0.048 \cdot Re_F^{0.6} \cdot Sc_F^{\frac{1}{3}} \quad (2)$$

$$PL_D = \frac{32 \cdot \mu_{D,av} \cdot v_{D,av}}{d_i} L \quad (3)$$

$$PL_F = \frac{32 \cdot \mu_{F,av} \cdot v_{F,av}}{D_i} L + \frac{150 \cdot (1-\varepsilon_D)^2 \cdot \mu_{F,av} \cdot v_{F,av}}{1.5^2 \cdot \varepsilon_D^3 \cdot d_{h,F}^2}(R_o - R_i) + \frac{1.75 \cdot (1-\varepsilon_D) \cdot \rho_{F,av} \cdot v_{F,av}^2}{1.5 \cdot \varepsilon_D^3 \cdot d_{h,F}}(R_o - R_i) \quad (4)$$

where Re is the Reynolds number, Sc is the Schmidt number and Sh is the Sherwood number. PL is the pressure loss, ε is the porosity and d_h is the hydraulic diameter of each channel. R_i is the inner radius of the fiber bundle (D_i is diameter), R_o is the outer radius of the fiber bundle and d_i is the inner fiber diameter (m). v is velocity, ρ is density and μ is the dynamic viscosity.

2.2. Model validation

The commercial FO HFMM used in this study (FP10130S3SI by Toyobo Company Ltd.) has not been tested yet under PRO conditions in an experimental plant. Experimental data in FO mode provided by the membrane manufacturer were used to validate the model [44]. This was done by fitting the coefficient A_0, taking into consideration the parameters shown in Table 3. The coefficient B could not be fitted, as the concentration at the FO outlet was not provided by Toyobo (only Q_p was available). The value of B was taken from a previous study that used a similar FO HFMM [45]. Information on porosity parameters (as unit fraction) of both the draw (ε_D) and feed (ε_F) sides were not available for the aforementioned HFMM, so the value of ε_D from a previous published study [46] for RO HFMM was used, and ε_F was assumed at 1.0. Similarly, S_f was taken from the published experimental study by Tanaka et al. [47]. The operating conditions were: $C_{D,in}$ = 58.5 g L^{-1}, $C_{F,in}$ = 0 g L^{-1} (NaCl), $p_{F,in}$ = 30 bar, $p_{D,in}$ = 10 bar, $Q_{D,in}$ = 0.6 m^3 h^{-1}, $Q_{F,in}$ = 3.4 m^3 h^{-1}, and Q_p = 2.37 m^3 h^{-1}. The obtained coefficient A_0 was 3.92 ×10^{-13} m Pa^{-1} s^{-1}.

Table 2
Summary information on studies about PRO using HFMMs.

Reference	Max. PD	System characteristics	Salinity gradient	Op. Conditions
Chou et al. [29]	20.9 W m^{-2} (Exp.)	$S_m = 1.36 \times 10^{-2}$ m^2 $A = 4.22 \times 10^{-12}$ m Pa^{-1} s^{-1} $B = 6.7 \times 10^{-8}$ m s^{-1} $S_f = 610$ μm	58.5-0.06 g L^{-1}	$\Delta p = 15$ bar
Sun et al. [30]	7.63 W m^{-2} (Exp.)	$A = 3.94 \times 10^{-12}$ m Pa^{-1} s^{-1} $B = 1.11 \times 10^{-7}$ m s^{-1}	$C_{D,in} = 58.5$ g L^{-1} FS: DI water	$p_{D,in} = 20$ bar $Q_{D,in} = 0.03$ m^3 h^{-1} $Q_{F,in} = 3.6 \times 10^{-3}$ m^3 h^{-1}
Higa et al. [31]	0.14 W m^{-2} (Exp.)	$S_m = 72$ m^2 $A = 2.5 \times 10^{-13}$ m Pa^{-1} s^{-1} $B = 8.05 \times 10^{-9}$ m s^{-1}	$C_{D,in} = 29.25$ g L^{-1} FS: Tap water	$p_{D,in} = 1.2$ bar $Q_{D,in} = 0.06–0.36$ m^3 h^{-1} $Q_{F,in} = 0.03–0.12$ m^3 h^{-1}
Kishimoto et al. [32]	1.6 W m^{-2} (Sim.)	$S_m = 65.6$, 70.5 m^2	$C_{D,in} = 35$ g L^{-1} FS: Pure water	$p_{D,in} = 10$ bar $p_{F,in} = 1.5$ bar
Aseffa et al. [33]	0.45 W m^{-2} (Sim.)	$S_m = 30.5$ m^2 $A = 1.11 \times 10^{-12}$ m Pa^{-1} s^{-1} $B = 3.7 \times 10^{-8}$ m s^{-1} $S_f = 635$ μm	36-0.34 g L^{-1}	$p_{D,in} = 14.89$ bar $p_{F,in} = 0.31$ bar $Q_{D,in} = 0.07$ m^3 h^{-1} $Q_{F,in} = 0.06$ m^3 h^{-1}
Matsuyama et al. [34]	2.8 W m^{-2} (Sim. & Exp.)	$S_m = 650$ m^2 $A = 2.05 \times 10^{-12}$ m Pa^{-1} s^{-1} $B = 5.5 \times 10^{-9}$ m s^{-1} $S_f = 1024$ μm	35-0.2 g L^{-1}	$p_{D,in} = 15$ bar $p_{F,in} = 2$ bar $Q_{D,in} = 2.4$ m^3 h^{-1} $Q_{F,in} = 1.26$ m^3 h^{-1}
Al-Zainati et al. [35]	Not specified (Sim.)	Two-stages $S_m = 63$ m^2 $A = 1 \times 10^{-12}$ m Pa^{-1} s^{-1}	DS: RO brine $C_{F,in} = 1$ g L^{-1}	Not specified
Low et al. [36]	9.1 W m^{-2} (Exp.)	Lab-scale	$C_{D,in} = 58.5$ g L^{-1} FS: DI water	$Q_{D,in} = 0.12$ m^3 h^{-1}
Low et al. [36]	2.5 W m^{-2} (Exp.)	Pilot-scale $S_m = 1.88$ m^2	$C_{D,in} = 58.5$ g L^{-1} FS: DI water	$p_{D,in} = 12$ bar
Al-Zainati et al. [37]	15 W m^{-2} (Sim.)	Multiple stages $S_m = 63$ m^2	292.2-1.16 g L^{-1}	Not specified

2.3. Simulation conditions and parameters of the used HFMMs

To upscale and simulate operating conditions on an industrial scale, a wide range of flow rates, similar to those used in RO, have been considered. This has been done taking into account the maximum and minimum inlet and outlet flow rates typically used in a PV with RO membrane modules. Table 4 shows the considered ranges of $C_{D,in}$, $p_{D,in}$, $Q_{D,in}$ and $Q_{F,in}$, and the values of T and FF used in the simulations. Limitations in terms of maximum flux recovery (R) and Q_p per HFMM were not established. All calculations were performed considering a PV of up to 3 HFMMs arranged in series. The decision to limit the number of elements in series to 3 is due to the high permeate production of each membrane module, which is due to its large active surface area. The higher the permeate production, the lower the FS output flow rate. When considering 4 modules in series, it was observed that very few operating points were chosen, as the minimum outflow restriction was not met. Therefore, a maximum of 3 elements in series was considered.

2.4. Performance evaluation

To estimate the net energy that can be generated from a single-stage full-scale PRO system, the specific enthalpy (h) at the inlet and outlet of the hydraulic turbine and pumps needs to be known. Devices including draw and feed pumps, an ERD (pressure exchanger and booster pump) and turbine form part of the process. Fig. 1 shows a flow diagram of the PRO plant, considering these mentioned devices. The power (P) of these elements was considered in this study. Fig. 1 also shows the direction followed by the draw and feed streams (PRO operating in co-current), and how the membrane elements are connected when more than 1 HFMM is considered. Based on the PRO system results, the power in the hydraulic turbine (P_{TB}), draw, booster and feed pumps (P_{DP}, P_{BP} and P_{FP}, respectively) are calculated through the equations shown in the second sub-section of the Supplementary Material. The net power (P_{net}) is determined through Eq. (5). The draw pump output pressure (input of the pressure exchanger) was 0.5 bar.

$$P_{net} = P_{TB} - P_{DP} - P_{BP} - P_{FP} \quad (5)$$

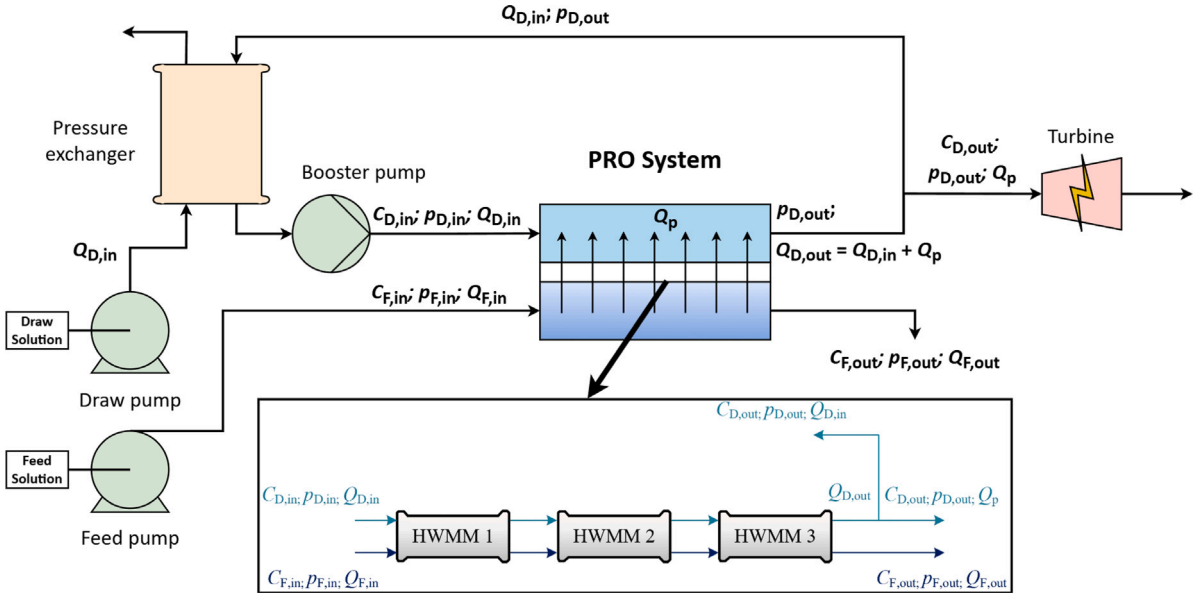

Fig. 1. Flow diagram of the evaluated PRO process.

Table 3
Parameters of 10-inch PRO HFMM and operating conditions for model validation.

Parameter	Value
A_0 (m Pa^{-1} s^{-1})	3.92×10^{-13}
B (m s^{-1})	1.5×10^{-8}
S_f (μm)	1024
S_m (m^2)	650
L (m)	0.68
H_D (m)	1.1×10^{-3}
H_F (m)	1.5×10^{-3}
d_i (m)	105×10^{-6}
R_i (m)	1.27×10^{-2}
R_o (m)	5.33×10^{-2}
ϵ_D	0.4
ϵ_F	1.0
FF	1.0
T (°C)	25
$C_{D,in}$ (g L^{-1})	58.5
$p_{D,in}$ (bar)	10
$Q_{D,in}$ (m^3 h^{-1})	0.6
$C_{F,in}$ (g L^{-1})	0
$p_{F,in}$ (bar)	30
$Q_{F,in}$ (m^3 h^{-1})	3.4
Q_p (m^3 h^{-1})	2.37

Table 4
Simulation parameters and operating ranges.

Parameter	Range or value
S_m (m^2)	650
FF	1.0
T (°C)	25
$C_{D,in}$ (g L^{-1})	30-180
$\Delta C_{D,in}$	30
$p_{D,in}$ (bar)	3-80
$\Delta p_{D,in}$	0.5
$Q_{D,in}$ (m^3 h^{-1})	3-16
$\Delta Q_{D,in}$	0.5
$C_{F,in}$ (g L^{-1})	0.5
$p_{F,in}$ (bar)	2
$Q_{F,in}$ (m^3 h^{-1})	3-16
$\Delta Q_{F,in}$	0.5

$$PD_{net} = \frac{P_{net}}{nS_m} \quad (6)$$

where the efficiency (η) of the hydraulic turbine is considered 85% in this case, η of the three pumps is assumed as 80%, and n is the number of HFMMs in series of the PRO system. To calculate the maximum PD, P_{TB} is used in Eq. (6).

3. Results and discussion

This section is divided into different sub-sections in which the effect of the different parameters studied ($C_{D,in}$, $p_{D,in}$, $Q_{D,in}$, $Q_{F,in}$ and n, by implication) on the performance of an industrial scale PRO system is analyzed considering a single stage.

3.1. The effect of $C_{D,in}$ on P_{net}

Fig. 2 shows the trend of the generated P_{net} with the HFMMs in series and different values of $C_{D,in}$. The most elevated values were obtained considering 3 HFMMs arranged in series (almost 5 kW for $C_{D,in}$ = 180 g L^{-1} and about 1.5, 2.7 and 4 kW for $C_{D,in}$ of 90, 120 and 150 g L^{-1}, respectively), as this is the maximum number of elements considered for the evaluated single-stage PRO system. As can be seen, for every step of $C_{D,in}$ the amount of generated P_{net} increases when increasing the number of HFMMs arranged in series from 1 to 3.

Fig. 3 shows the evolution of the power consumption of the pumps and the power generation by the turbine when varying $C_{D,in}$ for the operating conditions that maximize P_{net} with 3 HFMMs in series. The histogram also reflects that, for these optimal operating conditions, P_{TB} is greater than the sum of P_{DP}, P_{BP} and P_{FP} for at least $C_{D,in}$ = 60 g L^{-1}. For $C_{D,in}$ = 180 g L^{-1}, P_{TB} is above 7.2 kW, which meant a maximum PD of about 3.69 W m^{-2}. It can be compared to the results published in a previous study [10] in which the maximum PD was about 20 W m^{-2} for the same $C_{D,in}$ and 8 SWMMs arranged in series, but SWMMs with a lower S_m (15.53 m^2) were considered and the generation was lower (2.5 kW).

It can be stated that the net PD was always positive under the operating conditions shown in Tables 5–7, when $C_{D,in}$ was at least 60 g L^{-1}. In a previous work [10], positive PD was obtained only with 5, 6, 7 or 8 SWMMs in series for a $C_{D,in}$ of 60 g L^{-1} and S_m of 15.53 m^2. Matta et al. [20] obtained a net PD of 9.8 W m^{-2} with a salinity

Table 5
Operating conditions that maximize P_{net} with 1 HFMM for different values of $C_{D,in}$.

Parameter	$C_{D,in}$ (g L^{-1})					
	30	60	90	120	150	180
$p_{D,in}$ (bar)	9.5	20	30.5	40	49.5	57.5
$Q_{D,in}$ (m^3 h^{-1})	3	3	3	3	3.5	4
$Q_{F,in}$ (m^3 h^{-1})	3	3	4	5	6	6
R (%)	22.76	29.38	27.51	25.44	23.72	24.94
P_{TB} (W)	152.03	414.21	788.58	1194.65	1650.65	2011.62
P_{net} (W)	−164.88	39.34	284.19	563.65	828.23	1050.73

Table 6
Operating conditions that maximize P_{net} with 2 HFMMs in series for different values of $C_{D,in}$.

Parameter	$C_{D,in}$ (g L^{-1})					
	30	60	90	120	150	180
$p_{D,in}$ (bar)	10.5	21.5	32	42.5	53	62.5
$Q_{D,in}$ (m^3 h^{-1})	3	3	3	4	5	5.5
$Q_{F,in}$ (m^3 h^{-1})	3.5	5.5	8.5	11.5	13.5	14
R (%)	31.38	31.04	27.41	25.31	24.47	24.77
P_{TB} (W)	268.55	858.02	1740.54	2874.38	4043.56	4977.16
P_{net} (W)	−96.06	289.56	895.61	1620.16	2365.04	3001.46

Table 7
Operating conditions that maximize P_{net} with 3 HFMMs in series for different values of $C_{D,in}$.

Parameter	$C_{D,in}$ (g L^{-1})					
	30	60	90	120	150	180
$p_{D,in}$ (bar)	11	22	33	44	54.5	65
$Q_{D,in}$ (m^3 h^{-1})	3	3	3.5	4.5	5	5.5
$Q_{F,in}$ (m^3 h^{-1})	4	8.5	13.5	16	16	16
R (%)	35.51	30.96	27.49	27.80	29.83	30.97
P_{TB} (W)	361.13	1343.74	2831.66	4491.51	5934.80	7296.14
P_{net} (W)	−49.37	549.03	1552.67	2773.98	3957.41	4987.10

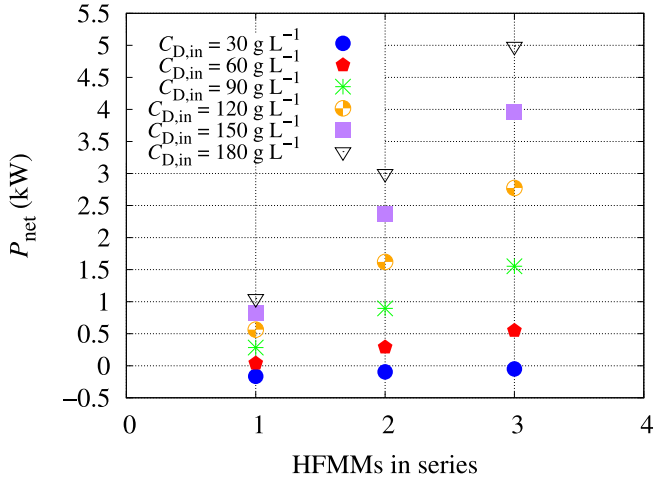

Fig. 2. Maximum P_{net} (kW) for different values of $C_{D,in}$ and 1 to 3 HFMMs arranged in series.

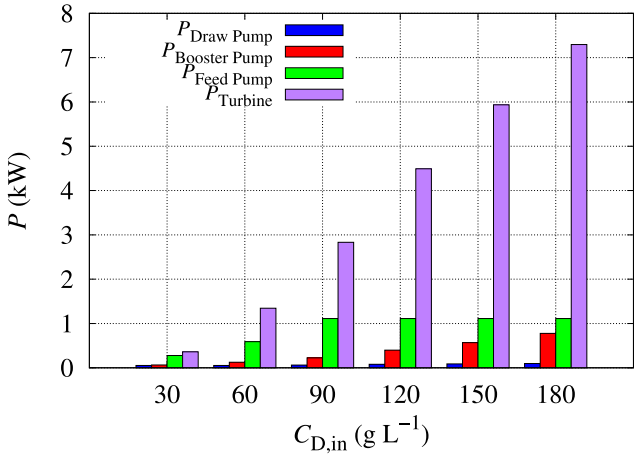

Fig. 3. Obtained P (kW) values of the different used devices as a function of $C_{D,in}$ for the operating conditions that maximize P_{net}, considering 3 HFMMs arranged in series.

gradient of about 125 g L^{-1} and a SWMM of 2 × 10^{-3} m^2. However, in the present work, for a salinity gradient of about 120 g L^{-1} and 3 HFMMs arranged in series, a net PD value of 1.42 W m^{-2} was obtained. This is because in the present study the membrane characteristics are different, with a higher S_f, a lower coefficient A, and a pump efficiency of 80% and a turbine efficiency of 85% were considered, whereas in the simulation study by Matta et al. [20] efficiencies of 100% were considered for the pumps and turbines. Furthermore, the aforementioned study did not consider a draw pump.

As can be seen in Fig. 2 and Table 7, the maximum P_{net} is 4987.1 W obtained with a $C_{D,in}$ of 180 g L^{-1} and 3 HFMMs in series (a net PD of 2.56 W m^{-2}).

3.2. The effect of $p_{D,in}$ on P_{net}

From Fig. 3, it can be seen that P_{DP} remained nearly constant despite the increase in $C_{D,in}$. This is because $p_{D,in}$ does not affect the consumption of the DP. Nevertheless, the necessary increase in $p_{D,in}$ due to $C_{D,in}$ variations did increase the consumption of the ERDs (booster

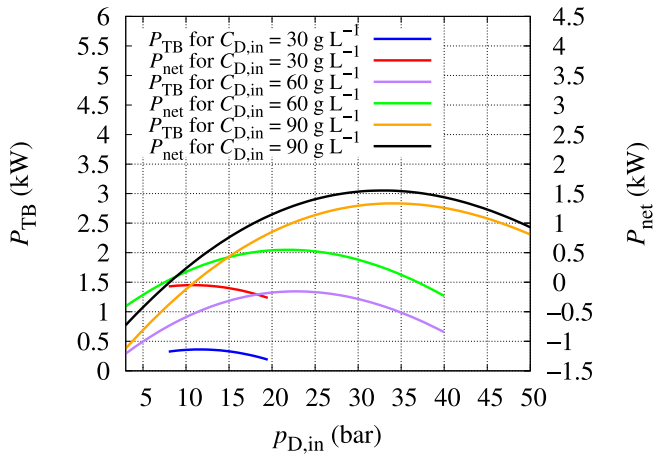

Fig. 4. Evolution curves of P_{TB} and P_{net} (kW) for different values of $p_{D,in}$, considering different $C_{D,in}$ values ranging from 30 to 90 g L^{-1} and 3 HFMMs arranged in series.

pump and pressure exchanger). This is why P_{BP} had an increasing trend, as did P_{FP} due to the enhancement of $Q_{F,in}$.

Fig. 4 shows the evolution curves of P_{TB} and P_{net} with $p_{D,in}$ for different $C_{D,in}$ values ranging from 30 to 90 g L^{-1}, with 3 HFMMs arranged in series in each case. Almost all curves present a quadratic trend in which P_{TB} and P_{net} increase up to a maximum value of $p_{D,in}$, and then both start to drop. The pressure of the maximum values of both P was lower than half of the value of $C_{D,in}$ but $p_{D,in}$ increased along with it. In some curves, the sections for which there are no P-values are due to the fact that the simulation results are out of the boundary conditions for that combination of $p_{D,in}$ and $C_{D,in}$.

Tables 5–7 support Fig. 4, as it is clearly shown the increase of $p_{D,in}$ with $C_{D,in}$ in order to obtain the maximum P_{net}, when considering from 1 HFMM to 3 HFMMs arranged in series. According to the results, to obtain P_{net} values equal or greater than 1.5 kW, $p_{D,in}$ cannot be less than 33 bar if 3 HFMMs are considered (and $C_{D,in}$ = 90 g L^{-1}) or less than 42.5 bar if 2 HFMMs are considered (and $C_{D,in}$ = 120 g L^{-1}). Matta et al. [20] determined that the maximum PD for a salinity gradient of about 125 g L^{-1} were obtained for a $p_{D,in}$ of about 50 bar. Tables 5, 6 and 7 show the $p_{D,in}$ values at which maximum P is obtained (40, 42.5, and 44 bar). For the salinity gradient of 120-0.5 g L^{-1}, the values are slightly below 50, which is reasonable since the number of elements arranged in series and the characteristics of the membrane influence this pressure values.

Fig. 5 shows the P_{net} variation with the change of $p_{D,in}$ and $Q_{D,in}$ (the values of P_{net} were obtained with 3 HFMMs arranged in series). As can be seen, there is a combination of pressure and flow rate values for which P_{net} reaches maximum values between 3.5 and 4 kW. For this net generation, $p_{D,in}$ ranged from 40 to 70 bar while the flow rate ranged between 3 and 8 m^3 h^{-1}. Under the conditions of Fig. 5 ($C_{D,in}$ = 150 g L^{-1}, $Q_{F,in}$ = 16 m^3 h^{-1} and 3 HFMMs in series), it should be noted that for $p_{D,in}$ under 35 bar and above 75 bar, P_{net} decreased below 3 kW (i.e., a loss of 25% of the generated power). The exact values for $p_{D,in}$ that maximize P_{net} in the studied ranges of $C_{D,in}$ and Q and 3 HFMMs in series can be verified through Table 7.

It is worth saying that the high $p_{D,in}$ that the HFMMs would be exposed to could tear them, consequently modifying the values of A and B and P_{net} along with them. This will be detrimental to the efficiency of the system and its viability.

3.3. The effect of $Q_{D,in}$ and $Q_{F,in}$ on P_{net}

Fig. 6 shows the obtained P_{net} for different ranges of $Q_{D,in}$ and $Q_{F,in}$. At low values of $Q_{D,in}$, the increase of $Q_{F,in}$ resulted in an enhancement of P_{net} up to 600 W, for the considered $C_{D,in}$ of 60 g L^{-1}, $p_{D,in}$ of 22 bar and with 3 HFMMs in series. In terms of flux recovery percentage (R), Table 7 shows that for a $Q_{F,in}$ of 8.5 m^3 h^{-1} and the considered C, p and n, R is 30.96%. Table 6 shows a similar value considering $C_{D,in}$ = 60 g L^{-1} but with a lower $Q_{F,in}$ of 5.5 m^3 h^{-1} and 2 HFMMs in series, giving also a lower P_{net} of 289.56 W. The R value for the maximum P_{net} obtained was 30.97% with a $Q_{F,in}$ of 16 m^3 h^{-1}.

It can additionally be seen in Tables 5–7 that R decreased almost every time $Q_{F,in}$ increased. To some degree, this is due to the increase of both $C_{D,in}$ and $p_{D,in}$ in accordance with what was shown in Eqs. (1)–(4) of the Supplementary material. Nevertheless, the gradual increase of $Q_{F,in}$ is sufficient to increase Q_p under every optimal operating conditions (the studied range of $C_{D,in}$) despite the decline of R. When $Q_{F,in}$ reached its maximum allowed value (16 m^3 h^{-1}), R always increased (from $C_{D,in} \geq$ 120 g L^{-1} in Table 7).

It is also interesting to note that, for $C_{D,in}$ of 30 and 60 g L^{-1}, $Q_{D,in}$ remained at the same value of 3 m^3 h^{-1} while considering 1, 2 and 3 HFMMs arranged in series. Then, $Q_{D,in}$ increased but at a slower pace (see Fig. 3, where the slower increase of P_{DP} can be seen). For the maximum P_{net} achieved with 3 HFMMs arranged in series (4987.1 W), $Q_{D,in}$ was only 5.5 m^3 h^{-1} although it was allowed to reach 16 m^3 h^{-1}. When comparing the value of $Q_{D,in}$ needed for the maximum P_{net} with 3 and then 2 HFMMs arranged in series, the same flow of 5.5 m^3 h^{-1} is required in order to obtain 3001.46 W with 180 g L^{-1} and 2 HFMMs in series.

The simulation results suggest that higher P_{net} could be reached with systems with more than one stage [37], but limiting operating conditions, including for example maximum and minimum flow rate in the draw and feed sides, should be taken into account. The flow rate could restrict the number of stages as it happens in RO process. By increasing the number of stages and therefore increasing the recovery of the system (solvent flow from the feed side to the draw side) we would be concentrating the feed solution more, which could lead to fouling problems. Operating with higher recoveries would force us to have a pre-treatment system for the feed water with a relatively high performance in order to try to extend the life of the PRO membranes as much as possible and to reduce the frequency of chemical cleaning, which would imply an increase in operation and maintenance costs.

4. Conclusions

The present study analyzed the influence of the parameters $C_{D,in}$, $p_{D,in}$, $Q_{D,in}$ and $Q_{F,in}$ in an industrial scale and single-stage PRO system with up to 3 HFMMs arranged in series. The operating conditions that maximize P_{net} were obtained and shown taking into account the aforementioned parameters and the number of HFMMs arranged in series (from 1 to 3). The maximum P_{net} achieved in this study was 4987.1 W (a net PD of about 2.56 W m^{-2}) considering a PV with 3 HFMMs arranged in series, surpassing the results of some previous works that used up to 8 SWMMs arranged in series or smaller HFMMs. To a certain extent, this was due to the large S_m of the selected membrane (650 m^2 of each membrane module). The increase in $C_{D,in}$ led to a higher required $p_{D,in}$, but causing the ERDs to consume more energy. The relationship between $Q_{D,in}$ and $Q_{F,in}$ with P_{net} and R was also studied. The maximum $Q_{F,in}$ considered (16 m^3 h^{-1}) was necessary to achieve higher P_{net} values only with 3 HFMMs arranged in series and for different $C_{D,in}$ values. The PRO system proved to be more sensitive to $Q_{D,in}$ than to $Q_{F,in}$, and was also quite dependent on fluctuations in $p_{D,in}$. However, the high flow rates caused the DP and FP to demand more energy, at the expense of P_{net}.

Industrial scale PRO systems considering one stage and HFMMs would be energetically practicable for concentration gradients in the range of 60 to 180 g L^{-1} and for the membrane properties considered in this study. Nevertheless, it is still necessary to compare the obtained

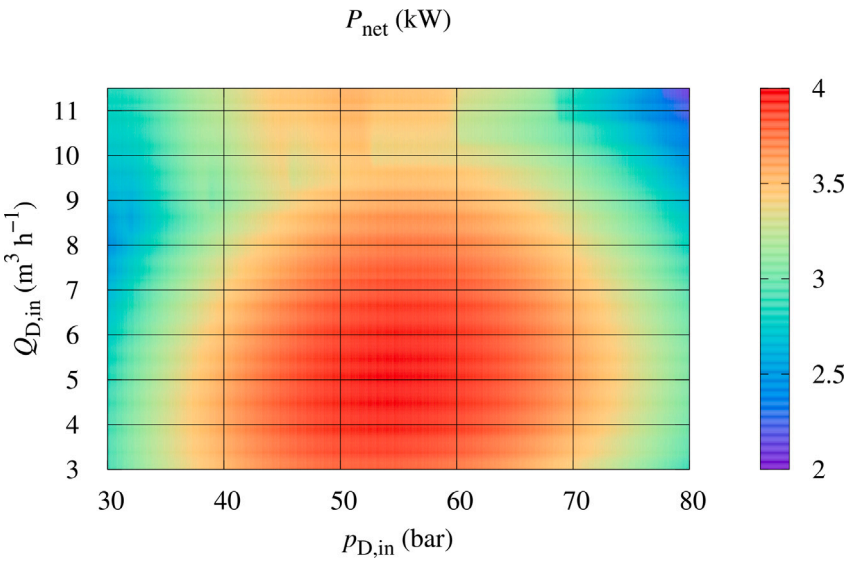

Fig. 5. P_{net} (kW) for different values of $p_{D,in}$ and $Q_{D,in}$, considering $C_{D,in}$ = 150 g L^{-1}, $Q_{F,in}$ = 16 m^3 h^{-1} and 3 HFMMs arranged in series.

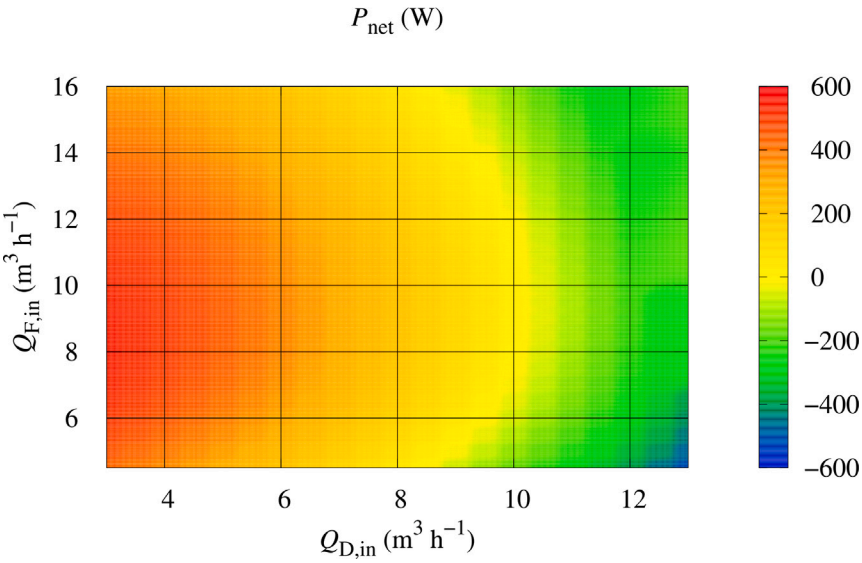

Fig. 6. P_{net} (W) for different values of $Q_{D,in}$ and $Q_{F,in}$, considering $C_{D,in}$ = 60 g L^{-1}, $p_{D,in}$ = 22 bar and 3 HFMMs arranged in series.

results with experimental ones in a full-scale PRO plant. The results obtained may vary due to the consideration of a membrane in perfect conditions and free of fouling. Membrane fouling, for example, would modify the values of A (decreasing) and B (increasing). In addition, no energy consumption of the pre-treatment stage for the feed streams has been considered, which would decrease the net power generation. It would also be useful to evaluate the performance of multi-stage PRO systems given the possibility of increasing energy production. Taking into account the state of the art of the current PRO technology and the operating conditions studied, this process could be applied for power generation in specific systems with high salinity gradients or in hybrid systems with other membrane technologies to improve the energy efficiency of the process. Unfortunately, and considering the current state of the art, the PRO technology with one stage is not feasible for massive power generation that would require large volumes of water such as sea and river where the salinity difference is approximately 30 g L^{-1}.

CRediT authorship contribution statement

D. Suárez-Alfonso: Writing – review & editing, Writing – original draft, Software, Methodology, Investigation, Data curation. **A. Ruiz-García:** Writing – review & editing, Validation, Supervision, Software, Resources, Project administration, Methodology, Investigation, Funding acquisition, Formal analysis, Conceptualization. **M. Khayet:** Writing – review & editing, Visualization, Validation, Supervision.

Declaration of competing interest

The authors declare the following financial interests/personal relationships which may be considered as potential competing interests: Daniel Suarez-Alfonso reports financial support was provided by University of Las Palmas de Gran Canaria. If there are other authors, they declare that they have no known competing financial interests or

personal relationships that could have appeared to influence the work reported in this paper.

Acknowledgments

This research is part of the project PID2022-138389OB-C32, funded by MCIN/AEI/10.13039/501100011033/FEDER, EU.

Appendix A. Supplementary data

Supplementary material related to this article can be found online at https://doi.org/10.1016/j.renene.2025.124344.

References

[1] M. Rastgar, K. Moradi, C. Burroughs, A. Hemmati, E. Hoek, M. Sadrzadeh, Harvesting blue energy based on salinity and temperature gradient: Challenges, solutions, and opportunities, Chem. Rev. 123 (16) (2023) 10156–10205, http://dx.doi.org/10.1021/acs.chemrev.3c00168.

[2] M. Bampaou, K. Panopoulos, An overview of hydrogen valleys: Current status, challenges and their role in increased renewable energy penetration, Renew. Sustain. Energy Rev. 207 (2025) 114923, http://dx.doi.org/10.1016/j.rser.2024.114923, https://www.sciencedirect.com/science/article/pii/S136403212400649X.

[3] M. Essalhi, A. Halil Avci, F. Lipnizki, N. Tavajohi, The potential of salinity gradient energy based on natural and anthropogenic resources in Sweden, Renew. Energy 215 (2023) 118984, http://dx.doi.org/10.1016/j.renene.2023.118984, https://www.sciencedirect.com/science/article/pii/S096014812300890X.

[4] J. Lee, Y. Shin, J. Kim, S. Hong, Feasibility and challenges of high-pressure pressure retarded osmosis applications utilizing seawater and hypersaline water sources, Desalination 581 (2024) 117578, http://dx.doi.org/10.1016/j.desal.2024.117578, https://www.sciencedirect.com/science/article/pii/S0011916424002893.

[5] M. Khayet, E. Aytaç, M. Essalhi, A. Cipollina, L. García-Fernández, J. Contreras-Martínez, C. García-Payo, A. Ruiz-García, A. Figoli, Elucidating the dynamics of salinity gradient energy research, Renew. Sustain. Energy Rev. 219 (2025) 115812, http://dx.doi.org/10.1016/j.rser.2025.115812, https://www.sciencedirect.com/science/article/pii/S136403212500485X.

[6] Y. Jiao, L. Song, C. Zhao, Y. An, W. Lu, B. He, C. Yang, Membrane-based indirect power generation technologies for harvesting salinity gradient energy - a review, Desalination 525 (2022) 115485, http://dx.doi.org/10.1016/j.desal.2021.115485, https://www.sciencedirect.com/science/article/pii/S0011916421005567.

[7] R.R. Gonzales, A. Abdel-Wahab, S. Adham, D.S. Han, S. Phuntsho, W. Suwaileh, N. Hilal, H.K. Shon, Salinity gradient energy generation by pressure retarded osmosis: A review, Desalination 500 (2021) 114841, http://dx.doi.org/10.1016/j.desal.2020.114841, https://www.sciencedirect.com/science/article/pii/S0011916420315198.

[8] T. Yang, T.-S. Chung, Novel thin-film nanocomposite hollow fiber membranes in modules with reduced reverse solute flux for pressure retarded osmosis, Chem. Eng. J. 450 (2022) 138338, http://dx.doi.org/10.1016/j.cej.2022.138338, https://www.sciencedirect.com/science/article/pii/S1385894722038219.

[9] S.N. Rahman, H. Saleem, S.J. Zaidi, Progress in membranes for pressure retarded osmosis application, Desalination 549 (2023) 116347, http://dx.doi.org/10.1016/j.desal.2022.116347, https://www.sciencedirect.com/science/article/pii/S0011916422008025.

[10] A. Ruiz-García, Power feasibility of single-staged full-scale PRO systems with hypersaline draw solutions, J. Water Process. Eng. 63 (2024) 105561, http://dx.doi.org/10.1016/j.jwpe.2024.105561, https://www.sciencedirect.com/science/article/pii/S2214714424007931.

[11] Y. Liang, Review of analytical and numerical modeling for pressure retarded osmosis membrane systems, Desalination 560 (2023) 116655, http://dx.doi.org/10.1016/j.desal.2023.116655, https://www.sciencedirect.com/science/article/pii/S0011916423002874.

[12] M.A.W. Khan, M.M. Zubair, H. Saleem, A. AlHawari, S.J. Zaidi, Modeling of osmotically-driven membrane processes: An overview, Desalination 573 (2024) 117183, http://dx.doi.org/10.1016/j.desal.2023.117183, https://www.sciencedirect.com/science/article/pii/S0011916423008159.

[13] C. Lee, S.H. Chae, E. Yang, S. Kim, J.H. Kim, I.S. Kim, A comprehensive review of the feasibility of pressure retarded osmosis: Recent technological advances and industrial efforts towards commercialization, Desalination 491 (2020) 114501, http://dx.doi.org/10.1016/j.desal.2020.114501, https://www.sciencedirect.com/science/article/pii/S0011916420302174.

[14] A. Achilli, J.L. Prante, N.T. Hancock, E.B. Maxwell, A.E. Childress, Experimental results from RO-PRO: A next generation system for low-energy desalination, Environ. Sci. Technol. 48 (11) (2014) 6437–6443, http://dx.doi.org/10.1021/es405556s.

[15] D. Attarde, M. Jain, K. Chaudhary, S.K. Gupta, Osmotically driven membrane processes by using a spiral wound module — modeling, experimentation and numerical parameter estimation, Desalination 361 (2015) 81–94, http://dx.doi.org/10.1016/j.desal.2015.01.025, https://www.sciencedirect.com/science/article/pii/S0011916415000442.

[16] S. Lee, Y.C. Kim, S.-J. Park, S.-K. Lee, H.-C. Choi, Experiment and modeling for performance of a spiral-wound pressure-retarded osmosis membrane module, Desalin. Water Treat. 57 (22) (2016) 10101–10110, http://dx.doi.org/10.1080/19443994.2015.1043494, https://www.sciencedirect.com/science/article/pii/S1944398624029059.

[17] G. O'Toole, L. Jones, C. Coutinho, C. Hayes, M. Napoles, A. Achilli, River-to-sea pressure retarded osmosis: Resource utilization in a full-scale facility, Desalination 389 (2016) 39–51, http://dx.doi.org/10.1016/j.desal.2016.01.012, pressure Retarded Osmosis, https://www.sciencedirect.com/science/article/pii/S0011916416300091.

[18] J. Benjamin, M.E. Arias, Q. Zhang, A techno-economic process model for pressure retarded osmosis based energy recovery in desalination plants, Desalination 476 (2020) 114218, http://dx.doi.org/10.1016/j.desal.2019.114218, https://www.sciencedirect.com/science/article/pii/S0011916419315115.

[19] N. AlZainati, S. Yadav, A. Altaee, S. Subbiah, S.J. Zaidi, J. Zhou, R.A. Al-Juboori, Y. Chen, M.H. Shaheed, Impact of hydrodynamic conditions on optimum power generation in dual stage pressure retarded osmosis using spiral-wound membrane, Energy Nexus 5 (2022) 100030, http://dx.doi.org/10.1016/j.nexus.2021.100030, https://www.sciencedirect.com/science/article/pii/S2772427121000309.

[20] S.M. Matta, M.A. Selam, H. Manzoor, S. Adham, H.K. Shon, M. Castier, A. Abdel-Wahab, Predicting the performance of spiral-wound membranes in pressure-retarded osmosis processes, Renew. Energy 189 (2022) 66–77, http://dx.doi.org/10.1016/j.renene.2022.02.125, https://www.sciencedirect.com/science/article/pii/S0960148122002749.

[21] Y.C. Kim, M. Elimelech, Adverse impact of feed channel spacers on the performance of pressure retarded osmosis, Env. Sci. Tech. 46 (8) (2012) 4673–4681, http://dx.doi.org/10.1021/es3002597.

[22] A. Ruiz-García, F. Tadeo, I. Nuez, Simulation tool for full-scale PRO systems using SWMMs, Desalination 541 (2022) 116025, http://dx.doi.org/10.1016/j.desal.2022.116025, https://www.sciencedirect.com/science/article/pii/S0011916422004805.

[23] B.A. Abdelkader, D.R. Navas, M.H. Sharqawy, A novel spiral wound module design for harvesting salinity gradient energy using pressure retarded osmosis, Renew. Energy 203 (2023) 542–553, http://dx.doi.org/10.1016/j.renene.2022.12.073, https://www.sciencedirect.com/science/article/pii/S0960148122018699.

[24] W. Ng, Y. Liang, G.F. Weihs, Quantifying the potential of pressure retarded osmosis advanced spacers for reducing specific energy consumption in hybrid desalination, J. Water Process. Eng. 55 (2023) 104197, http://dx.doi.org/10.1016/j.jwpe.2023.104197, https://www.sciencedirect.com/science/article/pii/S2214714423007171.

[25] A. Ruiz-García, F. Tadeo, I. Nuez, Role of permeability coefficients in salinity gradient energy generation by PRO systems with spiral wound membrane modules, Renew. Energy 215 (2023) 118954, http://dx.doi.org/10.1016/j.renene.2023.118954, https://www.sciencedirect.com/science/article/pii/S0960148123008601.

[26] M. Tagliavini, M.U. Babler, Simulation of spiral-wound pressure retarded osmosis for harvesting osmotic power: Module-level modeling and implications of feed pre-treatment, Desalination 574 (2024) 117184, http://dx.doi.org/10.1016/j.desal.2023.117184, https://www.sciencedirect.com/science/article/pii/S0011916423008160.

[27] O.A. AL-Musawi, A.W. Mohammad, H.B. Mahood, E. Mahmoudi, W.L. Ang, A.A.H. Kadhum, Energy comparison and cost estimation of pressure-retarded osmosis using spiral wound membrane, Desalin. Water. Treat. 320 (2024) 100732, http://dx.doi.org/10.1016/j.dwt.2024.100732, https://www.sciencedirect.com/science/article/pii/S1944398624202423.

[28] S. Yagnambhatt, S. Khanmohammadi, J. Maisonneuve, Demonstration of a real-time maximum power point tracker for salt gradient osmotic power systems, Appl. Energy 376 (2024) 124205, http://dx.doi.org/10.1016/j.apenergy.2024.124205, https://www.sciencedirect.com/science/article/pii/S0306261924015885.

[29] S. Chou, R. Wang, A.G. Fane, Robust and high performance hollow fiber membranes for energy harvesting from salinity gradients by pressure retarded osmosis, J. Membr. Sci. 448 (2013) 44–54, http://dx.doi.org/10.1016/j.memsci.2013.07.063, https://www.sciencedirect.com/science/article/pii/S037673881300639X.

[30] S.-P. Sun, T.-S. Chung, Outer-selective pressure-retarded osmosis hollow fiber membranes from vacuum-assisted interfacial polymerization for osmotic power generation, Environ. Sci. Technol. 47 (22) (2013) 13167–13174, http://dx.doi.org/10.1021/es403270n.

[31] M. Higa, D. Shigefuji, M. Shibuya, S. Izumikawa, Y. Ikebe, M. Yasukawa, N. Endo, A. Tanioka, Experimental study of a hollow fiber membrane module in pressure-retarded osmosis: Module performance comparison with volumetric-based power outputs, Desalination 420 (2017) 45–53, http://dx.doi.org/10.1016/j.desal.2017.06.015, https://www.sciencedirect.com/science/article/pii/S0011916416320033.

[32] M. Kishimoto, Y. Tanaka, M. Yasukawa, S. Goda, M. Higa, H. Matsuyama, Optimization of pressure-retarded osmosis with hollow-fiber membrane modules by numerical simulation, Ind. Eng. Chem. Res. 58 (16) (2019) 6687–6695, http://dx.doi.org/10.1021/acs.iecr.9b00139.

[33] H.T. Aseffa, D.K. Gautam, S. Subbiah, Optimization of pressure retarded osmosis process and estimation of indian blue energy capacity, Desalination 498 (2021) 114752, http://dx.doi.org/10.1016/j.desal.2020.114752, https://www.sciencedirect.com/science/article/pii/S0011916420314302.

[34] K. Matsuyama, R. Makabe, T. Ueyama, H. Sakai, K. Saito, T. Okumura, H. Hayashi, A. Tanioka, Power generation system based on pressure retarded osmosis with a commercially-available hollow fiber PRO membrane module using seawater and freshwater, Desalination 499 (2021) 114805, http://dx.doi.org/10.1016/j.desal.2020.114805, https://www.sciencedirect.com/science/article/pii/S0011916420314831.

[35] N. Al-Zainati, S. Subbiah, S. Yadav, A. Altaee, P. Bartocci, I. Ibrar, J. Zhou, A.K. Samal, F. Fantozzi, Experimental and theoretical work on reverse osmosis - dual stage pressure retarded osmosis hybrid system, Desalination 543 (2022) 116099, http://dx.doi.org/10.1016/j.desal.2022.116099, https://www.sciencedirect.com/science/article/pii/S0011916422005549.

[36] J.H. Low, J. Zhang, W.P. Li, T. Yang, C.F. Wan, F. Esa, M.S. Qua, K. Mottaiyan, S. Murugan, M. Aiman, A. Dhalla, T.-S. Chung, C. Gudipati, Industrial scale thin-film composite membrane modules for salinity-gradient energy harvesting through pressure retarded osmosis, Desalination 548 (2023) 116217, http://dx.doi.org/10.1016/j.desal.2022.116217, https://www.sciencedirect.com/science/article/pii/S0011916422006725.

[37] N. Al-Zainati, I. Ibrar, A. Altaee, S. Subbiah, J. Zhou, Multiple staging of pressure retarded osmosis: Impact on the energy generation, Desalination 573 (2024) 117199, http://dx.doi.org/10.1016/j.desal.2023.117199, https://www.sciencedirect.com/science/article/pii/S0011916423008317.

[38] A. Emdadi, P. Gikas, M. Farazaki, Y. Emami, Salinity gradient energy potential at the hyper saline urmia lake – zarrinehrud river system in iran, Renew. Energy 86 (2016) 154–162, http://dx.doi.org/10.1016/j.renene.2015.08.015, https://www.sciencedirect.com/science/article/pii/S0960148115302159.

[39] H.T. Madsen, S.S. Nissen, J. Muff, E.G. Søgaard, Pressure retarded osmosis from hypersaline solutions: Investigating commercial FO membranes at high pressures, Desalination 420 (2017) 183–190, http://dx.doi.org/10.1016/j.desal.2017.06.028, https://www.sciencedirect.com/science/article/pii/S0011916417304721.

[40] T.T. Tran, K. Park, A.D. Smith, System scaling approach and thermoeconomic analysis of a pressure retarded osmosis system for power production with hypersaline draw solution: A great salt lake case study, Energy 126 (2017) 97–111, http://dx.doi.org/10.1016/j.energy.2017.03.002, https://www.sciencedirect.com/science/article/pii/S0360544217303602.

[41] E. Bargiacchi, F. Orciuolo, L. Ferrari, U. Desideri, Use of pressure-retarded-osmosis to reduce reverse osmosis energy consumption by exploiting hypersaline flows, Energy 211 (2020) 118969, http://dx.doi.org/10.1016/j.energy.2020.118969, https://www.sciencedirect.com/science/article/pii/S0360544220320764.

[42] A. Janson, D. Dardor, M. Al Maas, J. Minier-Matar, A. Abdel-Wahab, S. Adham, Pressure-retarded osmosis for enhanced oil recovery, Desalination 491 (2020) 114568, http://dx.doi.org/10.1016/j.desal.2020.114568, https://www.sciencedirect.com/science/article/pii/S0011916420306305.

[43] S. Sarp, N. Hilal, Thermodynamic optimization of multistage pressure retarded osmosis (MPRO) with variable feed pressures for hypersaline solutions, Desalination 477 (2020) 114245, http://dx.doi.org/10.1016/j.desal.2019.114245, https://www.sciencedirect.com/science/article/pii/S0011916419320302.

[44] Toyobo Company Ltd, Toyobo MC Membrane Module for Forward Osmosis, https://www.toyobo-mc.jp/wordpress/wp-content/themes/toyobo_mc/assets/docs/products/en/brochure/brochure_fo_tmc.pdf.

[45] J. Minier-Matar, M. Al-Maas, A. Hussain, M.S. Nasser, S. Adham, Pilot-scale evaluation of forward osmosis membranes for volume reduction of industrial wastewater, Desalination 531 (2022) 115689, http://dx.doi.org/10.1016/j.desal.2022.115689, https://www.sciencedirect.com/science/article/pii/S0011916422001448.

[46] M.G. Marcovecchio, P.A. Aguirre, N.J. Scenna, Global optimal design of reverse osmosis networks for seawater desalination: modeling and algorithm, Desalination 184 (1) (2005) 259–271, http://dx.doi.org/10.1016/j.desal.2005.03.056, desalination and the Environment, https://www.sciencedirect.com/science/article/pii/S0011916405005710.

[47] Y. Tanaka, M. Yasukawa, S. Goda, H. Sakurai, M. Shibuya, T. Takahashi, M. Kishimoto, M. Higa, H. Matsuyama, Experimental and simulation studies of two types of 5-inch scale hollow fiber membrane modules for pressure-retarded osmosis, Desalination 447 (2018) 133–146, http://dx.doi.org/10.1016/j.desal.2018.09.015, https://www.sciencedirect.com/science/article/pii/S0011916417327753.